WAVE DRAG COEFFICIENT OF ELLIPTICAL FOREBODY SHAPES

SERDAREVIC-KADIC S., SOFTIC A. & RAZIC F.

Abstract: *The wave drag coefficient is a significant part of drag coefficient at speeds higher than the speed of sound and it depends on body shape and flow velocity. Elliptical cone and semi-ellipsoid in air flow with velocity from 1 to 2 Mach are studied by computational fluid dynamics. Fineness ratio of cone is chosen so that oblique shock wave is generated at the tip of the body. A semi-ellipsoid has a rounded tip so a detached bow shock wave is formed ahead of the body. Different ratios of semi-axis of elliptic base and different lengths of forebodies are considered and their influences to wave drag coefficient are analysed. It was confirmed that the wave drag coefficient decreases if the fineness ratio of forebody increases. The influence of semi-axis ratio of the elliptic base to wave drag coefficient is present for a cone in the entire interval of considered speeds and it is decreased with the fineness ratio increasing for a cone and for a semi-ellipsoid the influence is inversed.*

Key words: *Elliptical forebody, Mach number, Wave drag coefficient, Fineness ratio*

Authors´ data: Assistant Prof. Dr. Sc. Serdarevic-Kadic S[abina], Associate Prof. Dr. Sc. Softic A[lmira] & Assistant Prof. Dr. Sc. Razic F[aruk], Faculty of Mechanical Engineering, University of Sarajevo, Vilsonovo setaliste 9, Sarajevo 71000, Bosnia and Herzegovina, serdarevic@mef.unsa.ba, softic@mef.unsa.ba, razic@mef.unsa.ba.

This Publication has to be referred as: Serdarevic-Kadic, S[abina]; Softic, A[lmira] & Razic, F[aruk] (2023). Wave Drag Coefficient of Elliptical Forebody Shapes, Chapter 06 in DAAAM International Scientific Book 2023, pp.079-090, B. Katalinic (Ed.), Published by DAAAM International, ISBN 978-3-902734-39-6, ISSN 1726-9687, Vienna, Austria
DOI: 10.2507/daaam.scibook.2023.06

1. Introduction

Aerodynamic force is exerted on a body whenever there is a relative velocity between the body and the air. There are only two basic sources of aerodynamic force: the pressure distribution and the frictional shear stress distribution exerted by the airflow on the body surface. The pressure and shear stress act at each point on the body surface. The pressure exerted by the air at a point on the surface acts perpendicular to the surface at that point and the shear stress acts tangentially to the surface at that point. The distribution of pressure and shear stress represent a distributed load over the surface. The net aerodynamic force on the body is due to the net imbalance between these distributed loads as they are integrated over the entire surface (Anderson, 2017).

According to basic sources of drag formation, the drag of body can be divided into the following components: the pressure drag and the viscous drag on the wet surface of body, and drag due to underpressure on the dry surface of body (Serdarevic et al., 2022).

Pressure distribution over body is dependent on flow velocity and shape of body. If flow velocity is near or greater than the speed of sound, flow is characterized by the presence of shock waves across which the flow properties and streamlines change discontinuously. The shock wave is an almost explosive compression process, where the pressure increases almost discontinuously across the wave. The drag due to pressure distribution at wet surface of body in supersonic flow is called wave drag.

Every study of supersonic flow has to contain calculation of the shape and the strength of shock waves. The shape of the shock wave and complete flow field between the shock and the body depend on upstream Mach number and size and shape of the body (Anderson, 2017).

The desire to increase vehicle range and manoeuvrability has driven designers to consider non-axisymmetric body shapes. A noncircular cross-section may provide payload packaging benefits too.

Moxnes et al. (Moxnes, 2017) showed different novel analytical models for expected projected area and drag coefficient of irregular shaped bodies that tumble or rotate with the rotational axis normal to the velocity vector. They forecasted a model where the expected drag coefficient depends on the shape and Mach number. Murman (Murman, 2010) presented a method for predicting the drag of unconstrained bluff bodies from subsonic through supersonic flight conditions using analytic expressions.

The effect of various cross section of body (circular, square and hexagonal) on aerodynamic performances has been analysed by using Fluent CFD Code (Nallappan et al., 2015) and concluded that pressure coefficient value is low for body with hexagonal cross section for supersonic Mach numbers.

The MarcoPolo-R shape (cone with rounded tip) is investigated in a wide Mach number range within numerous wind tunnel tests and an aerodynamic database is built for the given capsule configuration (Gawehn et al., 2022). The experimental results are compared with numerical results in the study. Authors have noticed that the forebody part of axial force coefficient is highest around zero angle of attack and decreases with an increasing angle of attack.

The investigation has proven that the secondary shock system generated due to shock wave boundary layer interaction has a smaller influence on the drag coefficient than could have been expected.

The best way to analyse wave drag of noncircular body would be through numerical computations using code such as full Euler or Navier-Stokes, because the wave drag is more complicated than the other two components due to the fact that it is a function of the slope along the body surface as well as the area distribution (Moore, 2000). The ability to compute the pressure flow field for different configurations using Navier-Stokes computational techniques has been developed over the past few decades, so the Computational Fluid Dynamics (CFD) becomes an attractive alternative to expensive experiments.

Estimating wave drag coefficient of a forebody with an elliptical cross section at high speeds is the primary purpose of the paper. The secondary objective is to determine how much the axis ratio of the ellipse and fineness ratio of forebody affect to wave drag coefficient range.

2. Drag force and drag coefficient

A body in air flow is subjected to forces arising from the interaction of the flow and the body. Locally, the air flow exerts stresses on the body: normal stresses due to the pressure p and tangential wall shear stress τ_w due to viscosity. Once integrated over the entire surface, pressure and viscous contributions can be combined into the total force acting on the body. A component of total force acting in the direction of the upstream velocity is called drag force.

The external surface of body in air flow can be divided into the wet surface (the surface has contact with air) and the dry surface (region of separated air flow). According to basic sources of aerodynamic force formation, the drag force of a body can be divided into the following components:

$$D = D_{p_{wet}} + D_{\tau_{wet}} + D_{p_{dry}} \qquad (1)$$

where: $D_{p_{wet}}$ is the pressure drag on the wet surface of the body, $D_{\tau_{wet}}$ is the viscous drag on the wet surface of the body and $D_{p_{dry}}$ is the drag due to pressure on the dry surface of the body.

On the other side, the drag force is defined in terms of its drag coefficient as:

$$D = \frac{1}{2}\rho \cdot V^2 \cdot A_{ref} \cdot C_D \qquad (2)$$

where: ρ is freestream density, V is freestream velocity, A_{ref} is reference area and C_D is aerodynamic drag coefficient. Reference area is chosen to pertain to the given geometric body shape.

The aerodynamic drag coefficient of the body from equations (1) and (2) is the following:

$$C_D = C_{D_{p_{wet}}} + C_{D_{\tau_{wet}}} + C_{D_{p_{dry}}} \quad (3)$$

A major goal of theoretical aerodynamics is to calculate pressure distribution and shear stress distribution over the body surface for given body shape and freestream conditions.

2.1 Governing Fluid Flow Equations

The governing equations for an unsteady, compressible, three-dimensional, viscous flow are Navier-Stokes equations (Continuity equation, Momentum equations and Energy equation). These equations are a coupled system of non-linear partial differential equations, and hence are very difficult to solve analytically. There are five equations and six unknown flow-field variables: density ρ, pressure p, velocity $\boldsymbol{V}(u, v, w)$ and internal energy e. In aerodynamics, it is generally reasonable to assume the air is a perfect gas (which assumes that intermolecular forces are negligible). For a perfect gas, the equation of state is:

$$p = \rho R T \quad (4)$$

where R is the air gas constant and T is temperature. This provides a sixth equation, but it also introduces a seventh unknown - temperature. A seventh equation to close the entire system must be a thermodynamic relation between state variables. For a calorically perfect gas (constant specific heats), this relation would be:

$$e = c_v T \quad (5)$$

where c_v is the air specific heat at constant volume (Anderson, 1995).

Exact analytical solutions of the complete Navier-Stokes equations exist for only a few very specialized cases. Instead, the equations are frequently simplified by making appropriate approximations about the flow. In modern times, exact solutions of the complete Navier-Stokes equations for many practical problems can be obtained numerically, using various techniques of computational fluid dynamics (Anderson, 2017).

3. Computational Method

In this study, two different shapes of a body with an elliptical cross section are taken into consideration. Numerical simulations of the flow field around chosen bodies are obtained by the computational fluid dynamics software ANSYS Fluent in order to estimate the forebody drag coefficient due to pressure as a function of Mach number and fineness ratio.

The working fluid is air, an ideal gas, which is modified by compressibility and changes in thermophysical characteristics with temperature. Density and viscosity depend on the temperature, and specific heat at constant pressure and thermal conductivity are considered constants.

Pressure and temperature of air free flow correspond to parameters of air at sea level according to the standard atmosphere ICAO, $p = 101325\ Pa$ and $T = 288\ K$. The direction of airflow is assumed to be perpendicular to the maximum cross section of the body (reference area). Flow around the body is compressible and turbulent.

The numerical method that simultaneously solves the equation of continuity, the equation of momentum and the energy equation is used. This method is developed for high velocity compressible flows. The Spalart-Allmaras model is selected for turbulence modeling.

The governing equations are linearized implicitly. For a given variable, the unknown value in each cell is computed using a relation that includes both existing and unknown values from neighboring cells. Therefore, each unknown variable will appear in more than one equation in the system and these equations must be solved simultaneously to give the unknown quantities.

The first shape of the body was an elliptical cone. Two ratios of semi-width a and semi-height b of the elliptical base and three values of the fineness ratio of forebody λ are considered (Fig. 1).

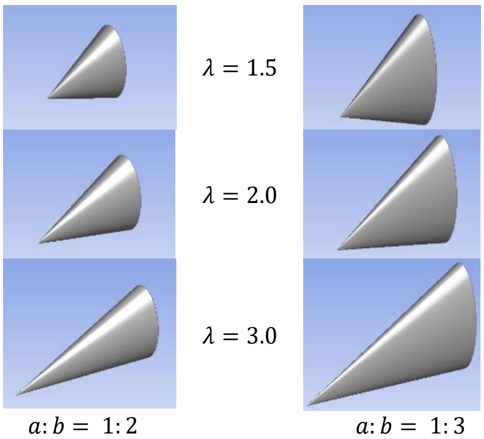

Fig. 1. Elliptical cones.

Fineness ratio is defined by:

$$\lambda = l/d_{eq} \tag{6}$$

where l is the length of the forebody and d_{eq} is the equivalent diameter.

The equivalent diameter is calculated as a diameter of a circle with the same area as the elliptical base by:

$$d_{eq} = \sqrt{4ab} \tag{7}$$

The second shape of the body was a semi-ellipsoid. The ratio of the semi-height and semi-width of an elliptic base and fineness ratio of the body (length of body in equivalent diameter) were the same as with the elliptical cone (Fig. 2.)

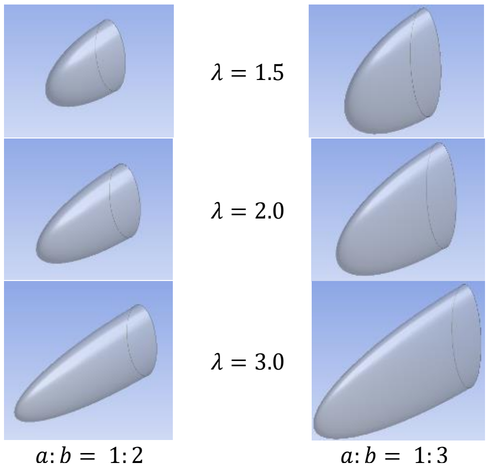

Fig. 2. Semi-ellipsoids.

3.1 Boundary Conditions and Mesh

Chosen bodies have two planes of symmetry and expected flow images are symmetrical to the two planes, so the simulations were made on one quarter of the body to decrease the time of calculation.

The computational domain is limited to the contour of the body, two symmetry planes and the outer boundary. The wall boundary, which is used to delimit the regions of fluid and solid, is set to the contour of the body. It is divided into a forebody wall and a base wall. Two symmetry planes are chosen as the boundary vertical symmetry plane and the boundary horizontal symmetry plane. Outer boundary of the domain is marked as a pressure far field boundary.

Discretization of the spatial domain is performed by unstructured non-uniform mesh. The sphere of influence is set around the body.

3.2 Verification of the Model

The verification of the computational model is done by the wave drag coefficient of the cone. Three lengths of a cone are considered for Mach numbers from 1 to 2.

The exterior boundary pressure farfield is set on $25d$ around the cone forebody and $35d$ from the base of cone. No slip conditions are set at the wall boundaries forebody and base. Boundary conditions are shown in Fig. 3.

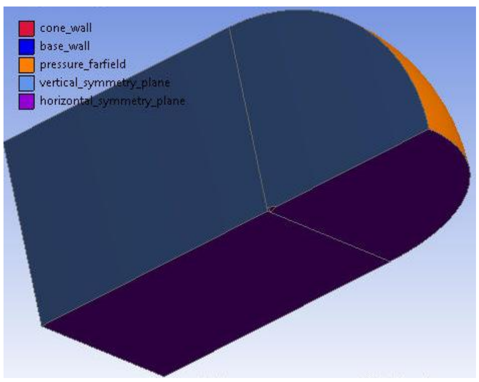

Fig. 3. Boundary conditions.

Mesh is created by the hex dominant method and the cone is surrounded by a sphere of influence as shown in Fig. 4.

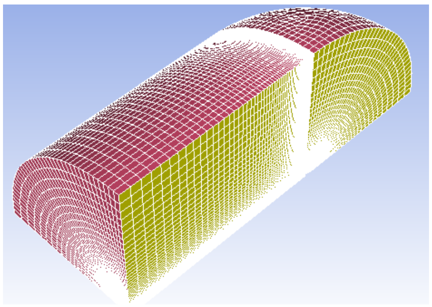

Fig. 4. Discretization of spatial domain.

Estimating values of wave drag coefficient are compared with theoretical calculation (Jankovic, 1979) and with experimental values for $\lambda = 3$ (Perkins, 1958). CFD results are shown by quads, results of theoretical calculations are shown by lines and experimental results are shown by stars (Fig. 5.).

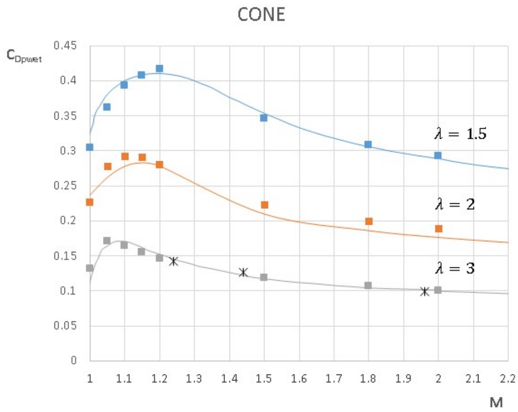

Fig. 5. Comparison of wave drag coefficient of cone.

The difference between theoretical calculation and the results of numerical simulation is less than 7% except for $M = 1$ when the difference is 13.5% for $\lambda = 1.5$, 4.6% for $\lambda = 2$, and 19.5% for $\lambda = 3$ (Table 1.).

Mach No.	Relative difference, %		
	$\lambda = 1.5$	$\lambda = 2$	$\lambda = 3$
1	13.48	4.64	-19.45
1.05	4.86	-6.14	-3.90
1.1	1.29	-5.04	3.18
1.15	-0.02	-2.58	2.81
1.2	-1.44	-0.46	2.93
1.5	1.64	-6.27	-1.54
1.8	-0.58	-6.82	-2.31
2	-1.71	-6.75	-1.003

Tab. 1. Relative difference between theoretical and CFD results.

The numerical results are in good agreement with the theoretical and experimental results which proves the accuracy of the numerical model.

4. Results and discussion

The results of simulation are grouped according to the shape of the body and the semi-axis ratio.

4.1 Elliptical Cone

For the cone with an elliptical base, the simulations are made for the following Mach numbers: 1, 1.05, 1.1, 1.15, 1.2, 1.5, 1.8 and 2.

The wave drag coefficient of elliptical cone with different semi-axis ratio of the base and for three different lengths of the body is shown in table 2.

Mach No.	Wave drag coefficient of elliptical cone, C_{D_W}					
	$a: b = 1: 2$			$a: b = 1: 3$		
	$\lambda = 1.5$	$\lambda = 2$	$\lambda = 3$	$\lambda = 1.5$	$\lambda = 2$	$\lambda = 3$
1	0.2943	0.2107	0.1250	0.2819	0.2082	0.1217
1.05	0.3566	0.2699	0.1675	0.3412	0.2615	0.1628
1.1	0.3879	0.2877	0.1619	0.3772	0.2818	0.1576
1.15	0.4032	0.2834	0.1497	0.3930	0.2771	0.1453
1.2	0.4070	0.2731	0.1405	0.3949	0.2636	0.1364
1.5	0.3349	0.2157	0.1151	0.3230	0.2089	0.1118
1.8	0.2982	0.1925	0.1031	0.2888	0.1870	0.1002
2	0.2834	0.1826	0.0976	0.2757	0.1779	0.0950

Tab. 2. Wave drag coefficient of elliptical cone.

The pressure field around an elliptical cone in the vertical and in the horizontal symmetry plane and static pressure distribution on the forebody for $M = 1.5$ is shown in Fig. 6.

The deflection angle of the air flow is equal to or lower than 30° for chosen semi-axis ratios of base and lengths of cone, so the attached shock wave is generated.

If the fineness ratio of the cone is increased, then the angle of generating shock wave attached to the tip of the cone is decreased for the same upstream Mach number. The pressure acting on the cone’s surface is decreased and drag coefficient has a lower value.

An elliptical cone with base semi-axis ratio 1:3 has a lower wave drag coefficient than an elliptical cone with base semi-axis ratio 1:2 for the same fineness ratio and for the same Mach number. The reference area of a cone with base semi-axis ratio 1:3 is approximate 1.5 times of reference area of a cone with base semi-axis ratio 1:2 and drag wave force of 1:3 cone is 1.44 times of drag wave force of 1:2 cone. Although the shock wave angle is higher for the cone with elliptic base 1:3, mean pressure on the surface of the cone is lower and it results with lower drag wave coefficient.

The chosen semi-axis ratio of base has a smaller influence on wave drag coefficient at higher fineness ratio of the cone.

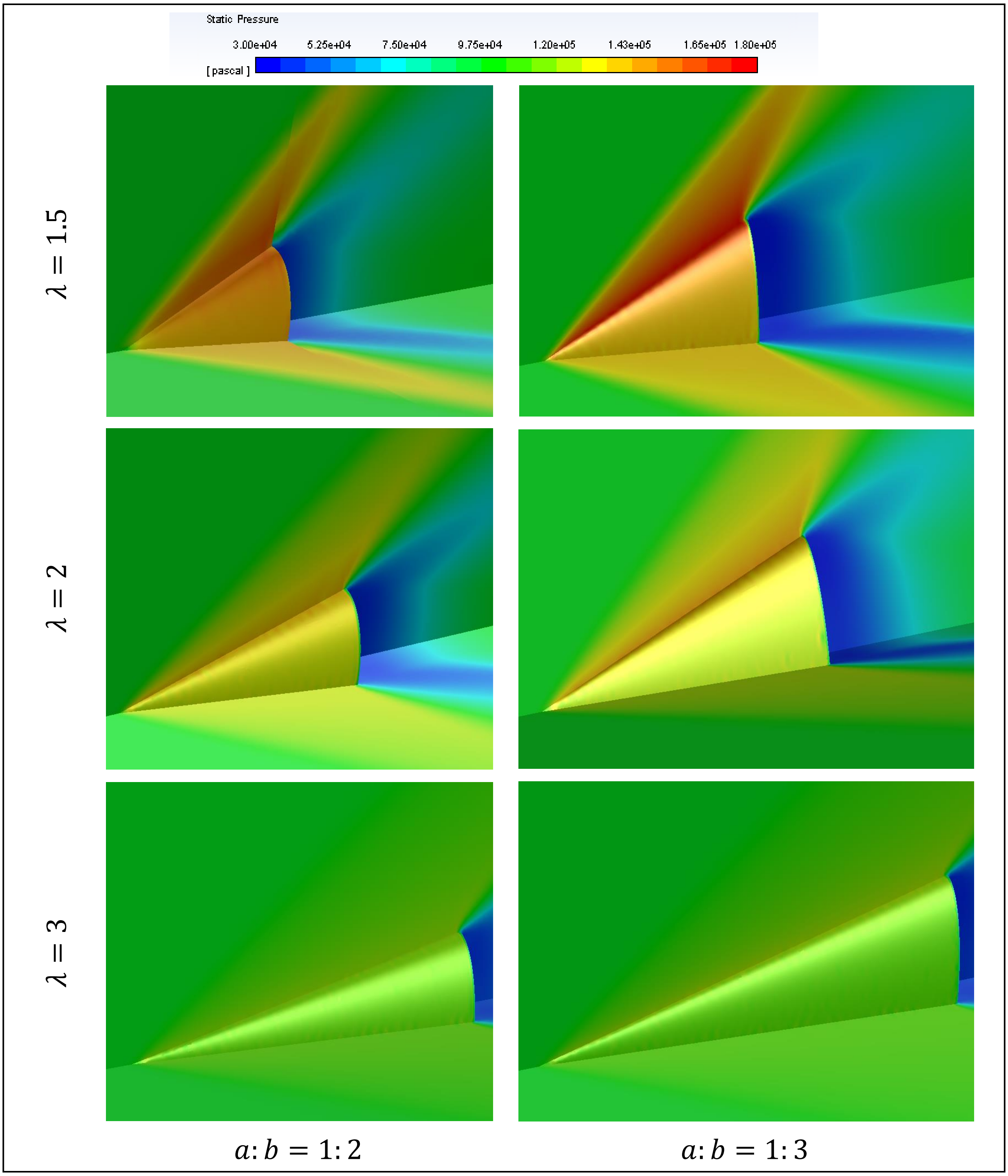

Fig. 6. Shock wave structure and static pressure distribution on the elliptical cone.

4.2 Semi-ellipsoid

For three-axis semi-ellipsoid, the simulations are made for the following Mach numbers: 1, 1.2, 1.3, 1.5, 1.8, 1.9 and 2. At a rounded forebody, like a semi-ellipsoid, detached bow shock wave is formed ahead of front surface.

The pressure field around a semi-ellipsoid in the vertical and in the horizontal symmetry plane and static pressure distribution on the forebody for $M = 1.5$ is shown in Fig. 7.

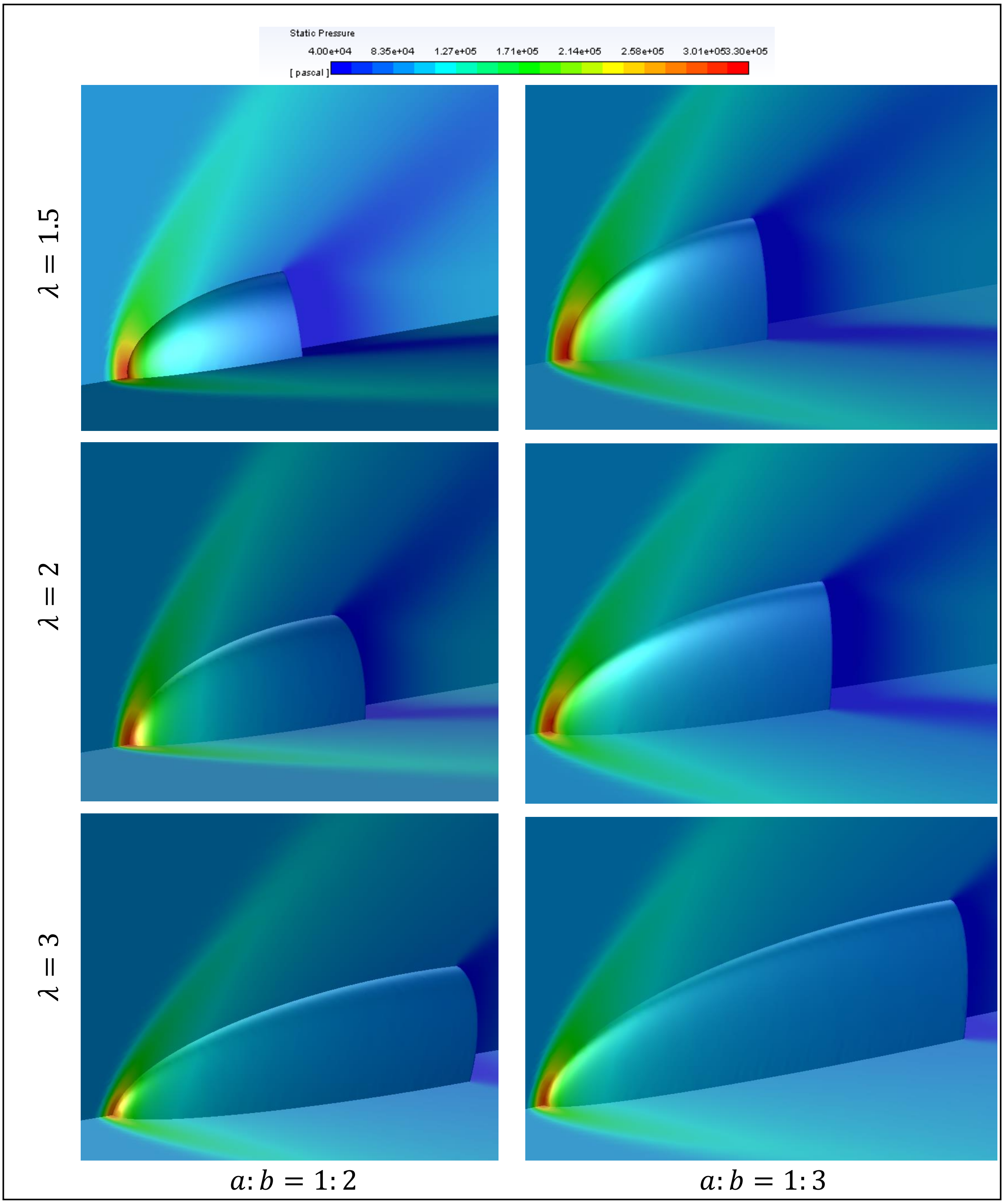

Fig. 7. Shock wave structure and static pressure distribution on the semi-ellipsoid

The wave drag coefficient of semi-ellipsoid with different semi-axis ratio of base and for three different lengths of the body is shown in table 3.

Mach No.	Wave drag coefficient of semi-ellipsoid, C_{D_W}					
	$a:b = 1:2$			$a:b = 1:3$		
	$\lambda = 1.5$	$\lambda = 2$	$\lambda = 3$	$\lambda = 1.5$	$\lambda = 2$	$\lambda = 3$
1	0.1063	0.0693	0.0351	0.1049	0.0676	0.0343
1.2	0.2548	0.1962	0.1269	0.2534	0.1951	0.1279
1.3	0.2870	0.2174	0.1394	0.2845	0.2175	0.1407
1.5	0.3197	0.2404	0.1501	0.3209	0.2420	0.1533
1.8	0.3413	0.2534	0.1565	0.3428	0.2567	0.1596
1.9	0.3446	0.2548	0.1567	0.3469	0.2596	0.1602
2	0.3459	0.2553	0.1569	0.3507	0.2602	0.1606

Tab. 3. Wave drag coefficient of semi-ellipsoid.

For the fineness ratio 1.5 and the velocity of the freestream up to 1.3 Mach, a semi-ellipsoid with the semi-axis ratio of base 1:2 has a higher value of the wave drag coefficient than a semi-ellipsoid with the semi-axis ratio of base 1:3. For the fineness ratio 2, this border is at 1.3 Mach and for the fineness ratio 3 a semi-ellipsoid with the base's semi-axis ratio 1:2 has higher wave drag coefficient than a semi-ellipsoid with the base's semi-axis ratio 1:3 only for $M = 1$.

For the velocities of the freestream up to 1.2 Mach and all chosen length, a semi-ellipsoid has a lower wave drag coefficient than a cone. If $M > 1.5$ a cone is a better shape of a forebody from the point of view of the forebody drag coefficient.

The semi-ellipsoid is a blunt body with a rounded tip. In high velocity flow ($M > 1$), the curved bow shock is generated in front of the body due to its shape. At the point of the shock wave at the axis of a semi-ellipsoid, the shock wave is normal to the upstream flow. Away from the axis of the body the shock wave becomes curved and weaker.

If the fineness ratio of a body is increased, bow shock becomes weaker and shock detachment distance is decreased for a given Mach number. Area of the rounded tip which is exposed to high pressure behind the shock wave is decreased and the forebody wave drag coefficient is decreased. If the fineness ratio of the forebody is doubled, the drag coefficient is decreased more than double for $M = 1.5$.

5. Conclusion

Numerical computations were made for bodies with an elliptical base at high speeds, from 1 to 2 Mach. Two shapes of a body: elliptical cone and three-axis semi-ellipsoid were considered. For every body two semi-axis ratios and three lengths were studied. There were 90 numerical simulations of flow around a body with an elliptical cross section, without verification of the model. The wave drag coefficient of a forebody was estimated and it is analysed in respect to the shape of the body, the semi-axis ratio of base, flow velocity and fineness ratio of the body.

Up to 1.5 Mach, a forebody shaped as a semi-ellipsoid is a more favourable shape than an elliptical cone from the point of view of the wave drag coefficient.

It was noted that the shape of forebody at transonic and supersonic speeds has significant influence to the forebody drag coefficient. The influence is related to the shape of the generated shock wave.

The influence of the semi-axis ratio of the base is decreased with the fineness ratio increasing for an elliptical cone and it is inverse for a semi-ellipsoid. The forebody drag coefficient of chosen bodies has a difference of less than 5% in a function of semi-axis ratio of base for a given Mach number and a given shape. Follow up research should deal with the analysis of body with elliptical cross section including shock wave boundary layer interaction.

6. References

Anderson, J. D. (1995). Computational Fluid Dynamics: The Basics with Applications, McGraw-Hill Companies, Inc., ISBN 0-07-001685-2, New York

Anderson, J. D. (2017). Fundamentals of Aerodynamics, McGraw-Hill Education, ISBN 978-1-259-12991-9, New York

Gawehn, T.; Schleutker, T. & Gülhan, A. (2022). Capsule aerodynamics and shock-wave boundary layer interaction (SBLI) in supersonic and transonic flow. Experiments in Fluids, Vol. 63, No. 3 (March 2022), pp. 61 (1-25), ISSN 1432-1114

Jankovic, S. (1979). Aerodinamika projektila, Masinski fakultet Univerziteta u Beogradu, ISBN, Beograd

Moore, F. G. (2000). Approximate Methods for Weapon Aerodynamics. American Institute of Aeronautics and Astronautics, ISBN 978-1-563-47399-9, Reston

Moxnes, J. F.; Frøyland, Ø.; Øye, I. J.; Brate, T. I.; Friis, E.; Ødegårdstuen, G. & Risdal, T. H. (2017). Projected area and drag coefficient of high velocity irregular fragments that rotate or tumble. Defence Technology, Vol. 13, No. 4 (June 2017), pp. 269-280, ISSN 2214-9147

Murman, S. (2010). Lift and drag behavior of unconstrained bluff bodies. The National Aeronautics and Space Administration (NASA/TM-2010-216406), Washington, D.C., USA

Nallappan, R.; Prasath, M.; Rajkumar, R. & Udhayan, K. (2015).Analysis of Missile Bodies with Various Cross sections and Enhancement of Aerodynamic Performance, International Conference on System, Science, Control, Communication, Engineering and Technology, T. Ramachandran (Ed.), pp. 115-119, ISBN 978-81-929866-1-6, India, August 2015, Association of Scientists, Developers and Faculties (ASDF, India), Coimbatore

Perkins, E. W.; Jorgensen, L. H. & Sommer, S. C. (1958). Investigation of the Drag of Various Axially Symmetric Nose Shapes of Fineness Ratio 3 for Mach Numbers from 1.24 to 7.4. National Advisory Committee for Aeronautics, Report No. 1386, Washington

Serdarevic-Kadic, S.; Softic, A. & Razić, F. (2022). Base drag of noncircular irregular shaped body at high speeds, Chapter 06 in DAAAM International Scientific Book 2022, pp. 075-084, B. Katalinic (Ed.), Published by DAAAM International, ISBN 978-3-902734-34-1, ISSN 1726-9687, Vienna, Austria